Vortex induced vibrations suppression for a cylinder with plasma actuators

F. Castro Hebrero, J. D'Adamo, R. Sosa, G. Artana

PII: S0022-460X(19)30684-4

DOI: https://doi.org/10.1016/j.jsv.2019.115121

Reference: YJSVI 115121

To appear in: *Journal of Sound and Vibration*

Received Date: 13 May 2019

Revised Date: 25 November 2019

Accepted Date: 25 November 2019

Please cite this article as: F. Castro Hebrero, J. D'Adamo, R. Sosa, G. Artana, Vortex induced vibrations suppression for a cylinder with plasma actuators, *Journal of Sound and Vibration* (2020), doi: https://doi.org/10.1016/j.jsv.2019.115121.

Vortex induced vibrations suppression for a cylinder with plasma actuators

F. Castro Hebrero[a,*], J. D'Adamo[a,b], R. Sosa[a,b], G. Artana[a,b]

[a] *Fluid Dynamics Laboratory, Buenos Aires University, Argentina.*
[b] *National Research Scientific and Technical Council, Argentina.*

Abstract

We propose the use of plasma actuators in order to control the vortex induced vibration phenomena (VIV) originated by an airflow around a rigid circular cylinder. The body was placed in a closed loop wind tunnel and mounted on elastic supports that allowed small oscillatory movements in the transverse direction with respect to the free stream. Our goal was to suppress the vibrations that naturally occurred in this configuration. To this end, two plasma actuators were disposed symmetrically on the surface of the cylinder along the span that transferred momentum to the fluid by means of a dielectric barrier discharge. The experiments were performed by varying the free stream velocity and the actuation parameters, which means voltage and frequency were kept constant throughout our experiments. We characterised the dynamics of the system for experimental conditions by involving a high reduced mass $m^* \approx O(10^3)$ and by considering a range of Reynolds numbers regarding the intermediate sub critical flow regime $1000 \lesssim Re \lesssim 10000$. The reduced velocities lied within the range of $4.50 < U_r < 6.25$. Our results show that the plasma actuators exhibit a large ability to suppress the VIV throughout the whole range of the experimental conditions tested. Complementary measurements undertaken with a particle image velocimetry (PIV) system enabled us to explain the outstanding performance observed.

*Corresponding author
Email address: fcastroh@fi.uba.ar, fcastroh@yahoo.com.ar (F. Castro Hebrero)

Keywords: circular cylinder, VIV, plasma actuators, plasma control, forced wakes

1. Introduction

The flow-induced vibrations of rigid bluff bodies have been largely investigated along the last decades; Nevertheless, most attention was given to the VIV of circular cylinders. This is, to some extent, not only due to the engineering importance of circular cross-section bodies but also because the dynamics of the wake of cylinders are considered as a reference flow to describe wakes of more complex bluff bodies. Since the landmark experimental measurements in [20] the practical significance of VIV has led to a large number of fundamental studies, many of which are discussed in comprehensive reviews (see e.g. Refs. Sarpkaya [39], Gabbai and Benaroya [22], Williamson and Goverdhan [50, 51], Bearman [6, 7], Sumer and Fredsoe [41], Mittal and Kumar [34]).

When Reynolds numbers, $Re = UD/\nu$, exceed a threshold value, close to 48, instabilities develop, leading to a time periodic flow configuration known as the Bérnard-von Kármán vortex street (BvK). Regarding the values of Reynolds number in proximity to this threshold, the wake is laminar and bi dimensional and it gradually becomes 3D as Reynolds number increases. Even though higher harmonics may develop when three-dimensional effects appear ($Re > 180$), the footprint of the fundamental 2D harmonic in the whole dynamics appears indicating its predominance in most of the cases [19]. VIV in rigid bodies occurs due to the fact that the shedding of vertices produce an oscillatory excitation to the structure. Depending on the characteristics of the supports, the system may oscillate due to lift or drag, or both type of forces. If the support restricts the movement to the transverse direction with respect to the free stream, the system oscillates only on account of lift forces. In general, the amplitude of transverse VIV, which can exceed a diameter in some cases, is greater than that of in-line VIV [27].

Bodies excited by vortices can experience a nonlinear phenomenon known as

lock-in when vortex shedding becomes synchronised with the natural frequencies of oscillation of the mechanical structure. This synchronisation can lead to an increase in the span wise correlation of the vortex shedding and consequently to a substantial amplification of the cylinders' vibrational response. When the vortex shedding frequency can be controlled, this lock-in phenomena between structure and shedding may be suppressed.

Over the years, controlling or suppressing VIV has drawn considerable attention to economic and technical interests such as enhancing safety or efficient operation, or life time of the structures affected by the VIV phenomena. In consequence, various VIV control devices are available. They can be classified into two major categories: passive, where no power input is required; and active, in which power input is required. For an extensive review on flow control actuators see, i.e. Cattafesta and Sheplak [12], Choi et al. [15], Gad-el Hak [23].

Passive VIV control is usually proposed by introducing geometrical changes to the bluff body with helical strake, shroud and tripping wires [24, 8, 43, 11, 31]. The main advantage of passive control methods is that they do not require energy input and, in consequence, they are easy to implement. It is difficult, however, to dramatically reduce the vortex-induced vibration with passive control. Furthermore, using these devices often produce an increase to the mean drag, as shown in Korkischko and Meneghini [31], Zdravkovich [53].

Active VIV control methods inject a small and tunable amount of energy to the flow and it seems to be a more attractive strategy, as forcing can be adjusted to the external modification of the conditions of the system. On one hand, vortex strength reduction strategies were applied to wakes in order to attenuate the resulting VIVs. Some examples are: moving surfaces [32], flush-mounted piezoelectric actuators [54], synthetic jets [44], pure suction [13] or blowing devices [40], windward-suction-leeward-blowing (WSLB) [45], rotational oscillations [18], travelling wave wall devices [52], and actuators based on Lorentz forces (MHD) [14].

On the other hand, VIV can also be mitigated by shifting the vortex shedding frequency away from the natural frequency of the body structures [46, 18]. One

possibility here is to consider devices that impose a periodic forcing to the flow. However, this strategy based on a synchronisation between forcing and shedding may be quite difficult. The flow dynamics, in general, may be driven by periodic external forces of reduced amplitude only within a narrow band of frequencies around the natural vortex shedding frequency. To introduce significant changes in the vortex shedding frequency, it may be more effective to propose another strategy based on a different concept. Rather than driving the flow to a forcing frequency, it may be more effective to produce modifications to the base flow that determines the instabilities that develop in the flow. It has previously been established that the base flow for cylinder wake studies is the averaged time flow [5]. Therefore, one possible strategy for VIV control is to force the flow in order to modify the main flow. In this research, we rely on this last strategy to suppress the VIV.

Since the pioneer works of Roth et al. [37], Artana et al. [3, 2] plasma actuators have rapidly developed over the last 30 years in the flow control community (see, for instance, the comprehensive reviews of Moreau [35], Corke et al. [16], Wang et al. [47]). However, according to our knowledge, only the work of Sari and Mureithi [38] has tried to control VIV by plasma actuation. On the contrary, in the aeroacoustic field, different authors proposed these devices to control the aerodynamic noise in geometries like cylinders [42, 26, 30], cavity flows [25] or flat plates [1].

Plasma actuators show unique properties in terms of flow manipulation, such as: momentum addition close to the wall, no moving parts, short command to action delays (of the order of the 1 μs) and high geometric versatility, allowing mounting on any surface exposed to the flow. Most of these actuators use non-thermal surface plasmas, in which the air flowing close to the wall of a body is weakly ionised. Due to the presence of charged particles within a highly non-uniform electric field and through a collisional mechanism, the plasma can create a body force close to the electrode surface. Consequently, this is a forcing without addition of mass. In some cases, the coupling flow-discharge is not only restricted to a collisional mechanism (heating by Joule effects of the fluid

particles flowing in proximity to the actuators), but they also produce slight modifications in physical properties, as density or viscosity, of these particles [28].

The different discharge configurations determine the stability of: the discharge, the electrode degradation, the electric force distribution or the energy consumption required to attain a given forcing. The most popular of these devices is the dielectric barrier discharge (DBD) actuator, which has been used to achieve control of diverse flows, exhibiting the following as strong advantages: a simple implementation, reproducible performances and relative robustness. Given that the forcing results quite localised a few millimetres from the border of the exposed electrode, this kind of discharge has largely been applied to different laboratory tests of flow control studies. With the DBD actuators the discharge is produced by applying a high voltage AC signal to a pair of electrodes that are separated by a dielectric layer. Typically, the voltage magnitude is of a few kV, the AC frequency is a few kHz, and the dielectric layer is of thickness $0.1 - 1$ mm. Under these conditions, stable surface plasma, consuming tens of watts per meter of electrode, can be easily created at atmospheric pressure. The amplitude control parameter can be directly adjusted in a relative small range by means of the high voltage AC signal amplitude. These actuators not only force the flow, but also the structure simultaneously. The ionic wind they induce, produces a reaction (thrust) that forces the structure in opposite direction to the induced flow. The phenomena is similar to the one well described in Loeb [33] for the ionic wind with a corona discharge wheel device. This force has been measured by different authors and its value is of the order of a few tens of 10^{-3} Nm^{-1}.

The objective of the present work is to analyse the ability of these DBD plasma actuators to suppress the VIV of a cylinder wake flow and to try to explain how this is produced.

2. Experimental setup

In the present investigation, we used a smooth hollow rigid cylinder made of polymethylmethacrylate (PMMA) with an external diameter of $D = 0.030$ m, a length of $L = 0.450$ m and a wall thickness of 3 mm. The mass of this cylinder was 0.204 kg. The cylinder was mounted inside the low turbulence *Tango Wind Tunnel* belonging to Fluid Dynamics Laboratory of Buenos Aires University [17] (Fig. 1). The wind tunnel square test section has a side width of $B = 0.455$ m and a total streamwise length of 0.910 m. The gap between the cylinder's ends and the lateral walls was of 2.5 mm (tunnel windows). There is a pair of holes that allow the cylinder to be linked with the elastic supports. No correction of results associated to blockage effect was done.

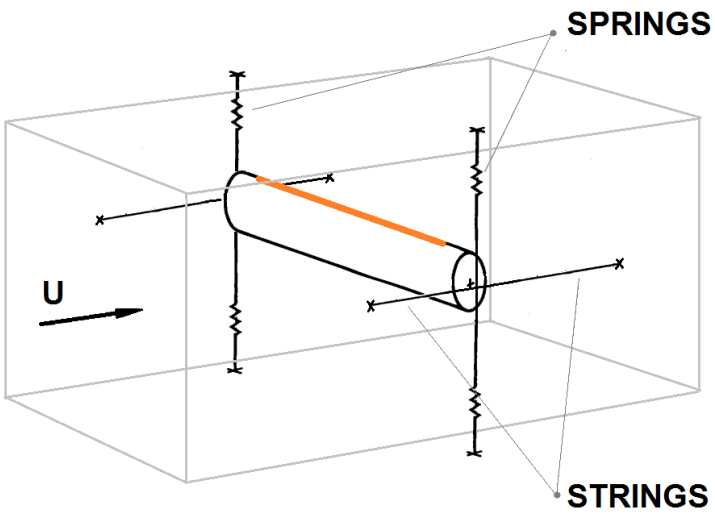

Figure 1: Representative scheme of the cylinder assembly inside the test area.

The flow velocity was varied between $U = 3.00 - 4.25$ ms^{-1} ($6000 < Re < 8500$) during the experiments. According to the classification of [49], this cylinder wake flow belongs to the so called Shear-Layer Transition Regime. This incoming free stream flow had fluctuations around the mean value lower than ± 2 %. The associated reduced velocity, $U_r = U/f_s^0 D$, where f_s^0 is the structure natural frequency, was thus varied between 4.50 and 6.25.

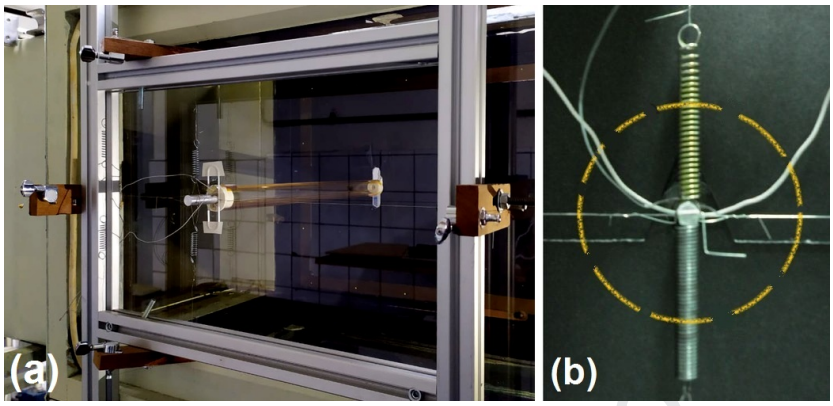

Figure 2: (a) Lateral wall of the section probe and the structure with the vertical pair of linear springs, horizontal guitar string and plasma electric wiring mounted outside the test section. (b) Details of the elastic supports in which is schematised the position of the cylinder inside the tunnel behind the lateral wall (shaded with a black sheet to avoid window reflections).

As for the range of Reynolds numbers considered, the expected Strouhal number is $St = f_{\rm vs}D/U \approx 0.208$ [21], with $f_{\rm vs}$ as the vortex shedding frequency. The flow we analysed has also been associated to a periodic detachment of transition eddies along the free shear layer. The frequency of formation of these eddies depend on Reynolds number. Typical frequencies of the transition eddies are close to 5 or 6 times the one of vortex shedding and, in our case, this corresponds to values that are larger than 150 Hz.

The cylinder was elastically mounted using four (two for each side) linear springs disposed outside the test section. Stressed strings was also used in order to restrain the cylinder movement, allowing only significant movements in the transverse direction with respect to the flow. This particular arrangement is suitably fitted in order to produce low structural damping (Fig. 2). The tunnel window possesses small grooves to allow the movement of the cylinder; fluid leaks are negligible.

2.1. Cylinder and flow dynamics

The transverse displacement of the cylinder was measured with an inductive displacement sensor with digital output (TURCK NI8-M18-LIU). The sensi-

tivity of the sensor in distance is of 0.040 mm. Its signal was captured by an oscilloscope (RIGOL 50 MHz, 4 channels) and the processing of the signal enabled us to obtain the frequency and the spectrum of energy regarding the cylinder's oscillations.

A 2D PIV acquisition system was further used to obtain the flow field at the mid-span of the cylinder. Image acquisition and PIV calculations were performed by using a LaVision system, composed of an ImagerPro 1200×1600 CCD camera with a 14-bit dynamic range and a two-rod Nd:YAG (15 mJ) pulsed laser synchronised with a customised PC using LaVision DaVis 7.1 software and the smoke was produced by atomising olive oil with a commercial smoke generator ($7 \cdot 10^{10}$ particle s^{-1} - generation rate). The experiment's field of view was of 175.5 mm $\times$ 234.0 mm (about $5.85D \times 7.8D$). While post-processing of the images with the PIV algorithm, this region was divided into interrogation cells of 16×16 pixels^2 with an overlapping of 50 % giving a spatial resolution of the vector fields of $0.078D$. The maximum sampling frequency of the system is about $14,8$ Hz and with the assumed $St \simeq 0.208$, we obtained $f_{vs} > 20$ Hz; in such a way, the flow field dynamics were sub-sampled on time. We have checked the correlation maps obtained with the PIV software and considered as outlier all point between the first and second peak, with a ratio lower than 1.2. The numbers of outliers in each snapshot were lower than 1 % and, in consequence, we stand for the idea that 3D effects do not contaminate this measurement significantly. When the flow is actuated with electrodes perpendicular to the streamwise direction, the 3D effects are expected to be less significant and it has already been demonstrated that in such cases the actuation promotes the synchronization of the roll up of the shear layer parallel to the spanwise direction [36]. We have also observed that the cylinder oscillates in a regime in which there is no tilt of the axis. Thus, even 3D effects can be present they are not strong enough to excite the cylinder in a mode in which the axis does not remain in an horizontal direction.

2.2. Plasma actuation characteristics

The plasma actuators geometry is shown in Fig. 3. The span of the actuator is 80 % of the cylinder's length. The electrodes were made of aluminium tape and the dielectric was made of 3 layers of Kapton tape of thickness 3×60 μm $= 180$ μm (Polyimide Film Tape with 6 kV of dielectric strength). The width of the insulated electrode (internal) is of 6 mm and as for the exposed electrode (external) it is of 10 mm. The actuators were disposed blowing in the downstream direction as it is schematically showed in Fig. 3. The downstream edges of the exposed electrodes were placed at $\pm 90°$ measured from the upstream stagnation point. With this setup, the electric thrust is negligible as forcing mechanism of the structure in the transverse direction.

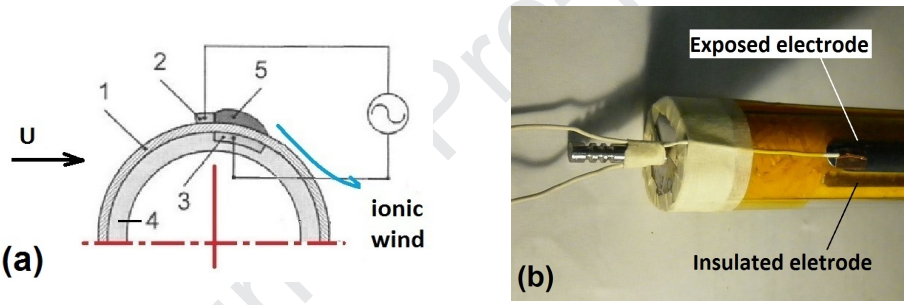

Figure 3: (a) Out of scale sketch: 1- Kapton, 2- Exposed electrode, 3- Insulated electrode, 4- Cylinder and 5- Plasma. (b) End of the cylinder and electrical terminals of the plasma actuator.

The electric circuit that excites the electrode was composed of a signal generator, an audio amplifier and an ignition coil. The voltage was set to $V_{\mathrm{ehd}} \approx 12$ kV$_{\mathrm{pp}}$ and the frequency of the AC signal was of $f_{\mathrm{plasma}} \approx 2$ kHz. In our experiments, these parameters of operation have always remained the same. The power consumption of the actuators is approximately of $20 - 25$ Wm^{-1}, so as for the aforementioned span, it is about $14.4 - 18.0$ W. Usually, only a fraction lower than 10% of this power is transformed into mechanical power supplied to the flow by the actuator [35].

With this setup there is a limit on the maximum voltage that can be used. This depends on the dielectric material considered and on its thickness. To

avoid an electrical breakdown of the dielectric film (Kapton) and, consequently, a possible damage of the actuator and/or of the power sources, we limited the voltage to a reasonable value. In similar setups, we observed that the use of higher voltage than the one we considered produced these undesired effects. The frequency of excitation was selected in order to have a quasi-continuous forcing. Forcing is produced in each cycle when discharge occurs. This only takes place in a limited fraction of the cycle and not during all its duration. By increasing the number of cycles per second, the repetition rate of actuation is increased and the forcing approximates much more to a continuous actuation. Therefore, a high frequency is of interest in this aspect. At the same time, the dielectric characteristics of the different materials and cables of the setup decrease their performance with increasing frequency values. Thus, taking into account these factors, we have selected the value of the frequency of our experiments.

2.3. Non dimensional parameters

Our mechanical system can be analysed as an elastically supported rigid circular cylinder of diameter D and of length L with one degree of freedom. When it faces a stationary and uniform flow of free stream velocity U, the cylinder can oscillate transversely as illustrated in Fig. 4.

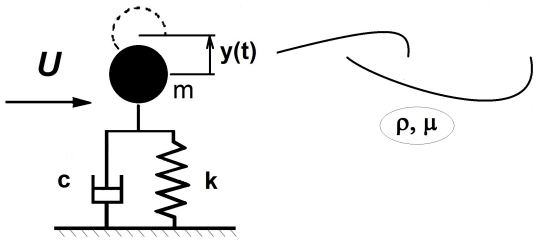

Figure 4: System configuration for an elastically-mounted, rigid cylinder in a uniform flow.

The dimensional in-plane cross-flow displacement $y \equiv y(t)$ of the structure is described by the following expression, which indicates the dynamics of a linear

oscillator

$$m\frac{\mathrm{d}^2y}{\mathrm{d}t^2} + c\frac{\mathrm{d}y}{\mathrm{d}t} + ky = F \ , \tag{1}$$

Where m is the total oscillating structural mass, c the structural damping, k the structural stiffness, $F \equiv F(t)$ the force in the transverse direction. The structural stiffness k of our setup was measured with a static calibration using reference masses. It was found to be 885 $\pm$ 20 Nm^{-1} per spring. On the other hand, the natural frequency (f_s^0) and the structural damping coefficient (ξ) were determined experimentally by means of a series of decay test in still air.

The model schematised in Fig. 4 is compatible with an identical and vertical in phase movement of both elastic supports of the cylinder. As opposite phase movement is not restricted with our set up we have determined the natural frequency oscillation in which both ends of the cylinder are not in phase (tilted mode). The frequency of the tilted mode was close to 35.5 Hz. The measured frequencies of oscillation in our experiments were rather far from this value, that is why the model proposed seems to be adequate as to describe the dynamics of our system.

Hence, the motion of the cylinder, y, that results from the coupling with the wake can be analysed in terms of simple variables: the amplitude A and frequency f_s of vibration. The dynamics of the flow brings as additional variable to the analysis, the dominant frequency of vortex shedding, f_vs. These variables, $A,\ f_\mathrm{s}\ ,f_\mathrm{vs}$, describe separately the characteristics of the fluid dynamics and of the structure, but are actually coupled.

This reads, in a general form

$$[A,\ f_\mathrm{s},\ f_\mathrm{vs}] = \mathcal{F}\left(m,\ c,\ k,\ U,\ \rho,\ \mu,\ D\right) \tag{2}$$

At this stage, because of the large number of parameters involved, some dimensional analysis is necessary. In dimensionless form,

$$\left[\frac{A}{D},\ \frac{f_\mathrm{s}}{f_\mathrm{s}^0},\ \frac{f_\mathrm{vs}}{f_\mathrm{s}^0}\right] = \mathcal{F}^*\left(\frac{UD\rho}{\mu},\ \frac{U}{f_\mathrm{s}^0 D},\ \frac{m}{\rho L \pi D^2/4},\ \xi\right) \tag{3}$$

The dimensionless groups on the right-hand side are the Reynolds number, the reduced velocity, the reduced mass (m^*) and the structural damping coefficient in still fluid ($\xi = c/4\pi m f_s^0$), where the natural frequency in still fluid, f_s^0, is defined as $\omega_s^0 = 2\pi f_s^0 = \sqrt{k/m}$.

The framework of our experimental study is given by the values adopted by these non-dimensional parameters.

Table 1 shows the experimentally obtained structural parameters. As it is usual for VIV studies undertaken with air flows, the reduced mass adopts relatively high values which in our case was $m^* = 523.5$ ($\approx 5 \cdot 10^2$). One can notice that although the system has a high reduced mass, the low damping ratio ξ leads to a relatively small Scruton number ($S_C = m^*\ \xi$) that is a key parameter in the observation of vortex shedding vibrations [10].The linearity of the damping coefficient was determined from several tests of amplitude decay.

Symbol	**Description**	**Dimension**	**Value**
k	structural stiffness	Nm^{-1}	$3540\ \pm\ 80$
f_s^0	natural frequency	Hz	$22.7\ \pm\ 0.5$
ξ	damping coefficient	–	$8.3\ \pm\ 0.5\ (\cdot\ 10^{-3})$

Table 1: Structural parameters

The vortex shedding frequency appears in Eq. (1) through the forcing term F incorporating a time depending on the excitation of the structure associated to the flow. There may be other frequencies of excitation of the structure associated to the flow. The transition eddies may also excite the structure but these vortices imply a much lower strength to one of the vortex shedding, and they also have an associated frequency much larger than the one of interest in our analysis. Thus, in a first analysis, their effect can be disregarded.

Moreover, in regard to the cases in which a control is proposed, plasma actuation forces the flow but this occurs only when discharge takes place. This corresponds to a limited part of the electric excitation of the cycle of the signal. In addition, the discharge may be considered as a pulsed forcing that takes place

recursively with frequency f_{plasma} but that it is not continuous. This actually introduces a forcing to the flow under a cyclic behaviour. Measurements of spectra of velocities belonging to different forced flows, in proximity to actuation with this kind of actuators, show, in general, peaks in agreement with this frequency of excitation [9]. We stand for the idea that it is of utmost importance in order to analyse if this frequency plays a significant role in our study or not. In order to achieve this, it is convenient to define two other non dimensional parameters f_{plasma}/f_s^o and $f_{\text{plasma}}/f_{\text{vs}}$. In our case, both ratio are quite far from unity ($f_{\text{plasma}}/f_{\text{s}}^o \sim f_{\text{plasma}}/f_{\text{vs}} \sim 100$). Thus, the resonance of the structure is quite far from the frequency of excitation that the actuator produces and instabilities of the flow that may be excited by the forcing also have quite lower values. So, we can conclude that the influence of the forcing's "high" frequency will not significantly be observed in the "slow" dynamic behaviour of the system analysed.

In summation, in our study D, L, m, c and k are constant (therefore with fixed values of ξ and m^*) and changes in the natural VIV phenomena can be achieved only as a consequence of modifications in the uniform fluid stream.The forcing parameters are also kept constant. Hence, the characteristics of the dynamics will be governed only by two non-dimensional numbers, the Reynolds number (Re) and the reduced velocity (U_r).

3. Results

3.1. Transverse Cylinder oscillations

Figure 5a) shows a typical signal obtained with the displacement sensor and Fig. 5c) shows the associated Fourier energy spectrum. In all the experiments the transverse displacement amplitude of the cylinder was obtained as the root mean square of the displacement signal ($A \equiv A_{\text{rms}}$), and the frequency of the cylinder oscillations (f_{s}) was obtained from the Fourier frequency spectrum of the signal. The recorded signal shows a high frequency signal whose amplitude is modulated by a low frequency. Figure 5b) shows a *linear-log* graph zoom of

the Fourier energy spectrum. The spectrum shows that in the cylinder oscillation there exists a dominant frequency but there also may appear a significant contribution to the signal given by oscillation modes (first peak) in addition to another frequency in proximity to the dominant one (secondary peak). Figure 5c) shows a global observation of the spectrum. The third peak appearing at proximity of 35.5 Hz corresponds to the tilted movement mode. Finally, harmonics of the first two peaks appear close to 44.5 Hz.

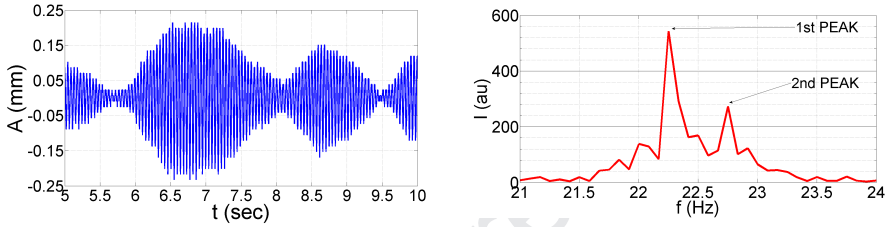

a) b)

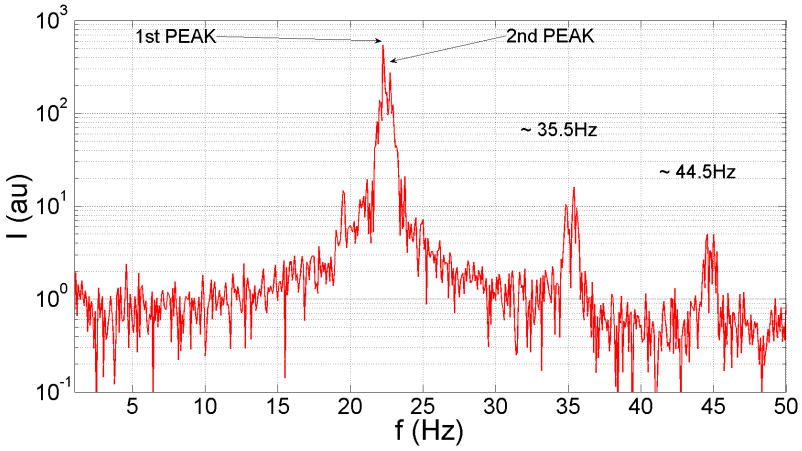

c)

Figure 5: $U \approx 3.85$ ms^{-1}. a) Signal obtained with the displacement sensor. *Sampling* $= 1000$ Hz and $t_{\text{total}} = 7$. b) *linear-linear* spectrum graph. 1^{st} Peak: $f_1 = 22.25$ Hz and $E_1 = 542$ a.u. 2^{nd} Peak: $f_2 = 22.75$ Hz and $E_2 = 270$ a.u. c) *linear-log* spectrum graph. Fundamental frequency of tilted movement ~ 35.5 Hz and first harmonic ~ 44.5 Hz.

Figure 6 shows the dimensionless amplitude ($A^* = A/D$) of the oscillations

of the cylinder in terms of reduced velocity for the *Plasma on* (actuated or forced) and *Plasma off* cases respectively. Within our experimental conditions, the cylinder displacements have shown a relative dispersion of results among experiments. In order to find representative results we have performed more than thirty experiments for the *Plasma off* case. We have plotted the average values of A^* for each reduced velocity and their scatter about that mean (*Plasma off - Std*). This figure shows that no vibrations occur for $U_r < 4.75$. On increasing U_r, the amplitude rises sharply to a maximum amplitude value. The maximum response is confined to a quite narrow reduced velocity range, $4.75 < U_r < 5.5$, which is typical of moderate to high-mass-ratio VIV and the maximum is centred upon $U_r \approx 5.15 \approx 1/St$ [10]. By further increasing the velocity of the free airstream, and in consequence of the reduced velocity, we observed that a second local maximum may occur in proximity to the value of $U_r = 6$.

Let's also remark that for the cases close to resonance $U_r \approx 5$ it is reasonable to consider an approximation expressed in [50] to estimate the lift coefficient C_L represented in Eq. (4).

$$C_L = \frac{A}{D} 4\pi^3 (1 + m^*) St^2 \xi \tag{4}$$

In this sense, regarding the measured parameters and displacements, $C_L \approx 0.7$, we are referring to a value that can be compared with experimental data from the literature (see i.e. [53]).

In [48] the dependency of circular cylinders VIV on their mass ratio (within the range $1 < m^* < 50$) and for a relative low Reynolds numbers range $50 < \mathrm{Re} < 400$ was studied. The authors have found secondary, or super-harmonically excited, responses occur for the higher mass ratios considered. Even though the ranges of Reynolds numbers and mass ratio considered in our work are not the same as in in [48], we consider that the second local maximum observed could be associated to a secondary (or super-harmonically excited) response.

Figure 7 a) shows the non-dimensional frequency response ($f^* = f_s/f_s^0$) for a typical *Plasma off* case in which the frequencies f_s were obtained by identifying

the most energetic peaks in the energy spectra of the cylinder's displacement signal and then through dividing by f_s^0 (resulting the circles symbols in Fig. 7 a)). It can be seen that the measured mean frequency of the oscillation of the cylinder corresponds to the natural frequency of the structure still in fluid ($f^* \approx 1$ thus $f_s \approx f_s^0$).

For all the spectra, we have also selected a second mode of oscillation having an associated peak with a value exceeding 10% of that of the most energetic called secondary peak ($E_2/E_1 \gtrsim 0.10$). An example of this secondary peak was represented in Fig. 5 c). These peaks occur for U_r values quite away from the natural frequencies of the structure. The second mode is signalled with square symbols considering a case taken as reference in Fig. 7 a). A linear fitting of the different values of these second peaks obtained for all the experiments is proposed in Fig. 7 b). The fitting gives a $St \approx 0.198$ quite close to Strouhal number $St \approx 0.208$ quoted in the literature for a fixed cylinder under this flow conditions [21].

Considering now the *Plasma on* case, the plasma actuation flattens the spectrum energy and cancels the oscillations for all the different velocities tested as it can be observed in Fig.6. It is important to mention that contrary to what was observed for the *Plasma off* case, when the flow is actuated, the curves $A^*(U_r)$ show a very repetitive behaviour. Thus, under these conditions, the amount of data required to characterise the flow control effect was considerably lower than that for the non-actuated case. In order to have a better insight on the physics that can explain this outstanding result, we performed PIV experiments to have access to the fluid dynamics.

In [48] the dependency of circular cylinders VIV on their mass ratio (within the range $1 < m^* < 50$) and for a relative low Reynolds numbers range $50 < Re < 400$, was studied. As for the cases with the higher values of mass ratio, it has been found not only a primary response region normally associated with VIV but also a secondary region was observed in the same sense as we did first. Even though the ranges of Reynolds numbers and mass ratio are not the same in both cases, the results illustrated in Fig. 6 show a similar behaviour as the

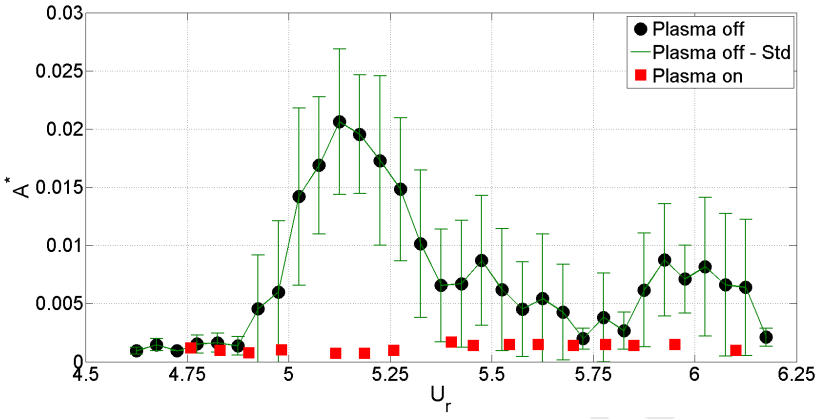

Figure 6: Dimensionless amplitude A^* vs reduced velocity U_r.

one observed in [48].

3.2. PIV measurements

PIV measurements were made for the flow in the range of reduced velocities $U_r \in [5.2, 5.5]$, considering the *Plasma on* and *Plasma off* cases. Each test was undertaken with the acquisition of 510 successive snapshots, suitable to achieve statistical convergence. Assuming ergodicity, the average time $\langle \mathbf{u}(\mathbf{x}) \rangle$ and the fluctuation intensity $\langle u_i' u_j'(\mathbf{x}) \rangle^{1/2}$ of the velocity fields $\mathbf{u}(\mathbf{x}) = (u_x(x,y), u_y(x,y))$ were determined respectively as follows:

$$\langle \mathbf{u}(\mathbf{x}) \rangle = \frac{1}{N} \sum_{i=1}^{N} \mathbf{u}(\mathbf{x}, t_i) \tag{5}$$

$$\langle u_i' u_j'(\mathbf{x}) \rangle^{1/2} = \left[\frac{1}{N} \sum_{i=1}^{N} \left(u_i(\mathbf{x}, t_i) - \langle u_i \rangle \right) \left(u_j(\mathbf{x}, t_i) - \langle u_j \rangle \right) \right]^{1/2} \tag{6}$$

Figure 8 shows the time average velocity fields, for the *Plasma on* and *Plasma off* cases, for $U_r = 5.2$ and $U_r = 5.5$ respectively represented by streamlines and velocity contours. We find it important to recall that at the considered Reynolds numbers, the BvK vortex street remains the same as the dominating flow coherent structure. In the near wake, where the flow is decelerated after

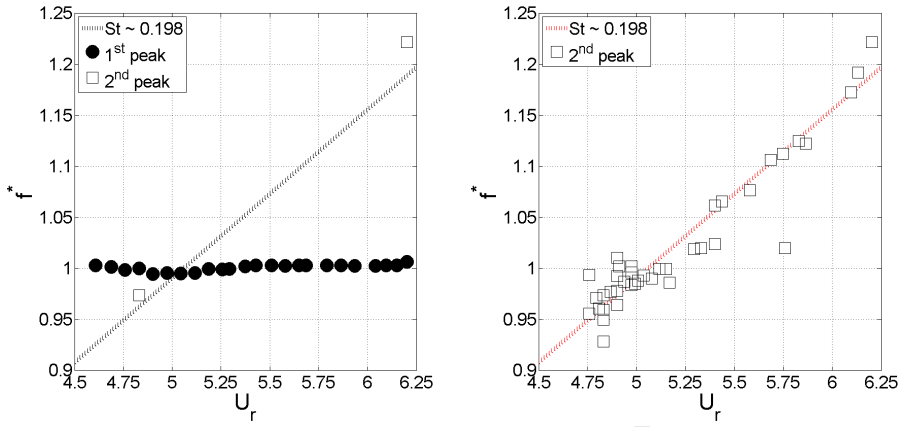

a) b)

Figure 7: Dimensionless frequency f^* vs reduced velocity U_r. a) Typical *Plasma off* case. Black circles: most energetic peaks in the spectra; white squares: second peaks in the spectra; b) Straight line: best linear fit to observe second peaks in white squares for all the *Plasma off* cases.

the detachment, a main re-circulation region that encloses two counter-rotating vortices can be defined. It is possible to define this region as having a re-circulation length of ℓ_m, the distance between the cylinder and the furthest downstream point where the streamwise velocity is $u_x = 0$. For the unforced flow, Fig. 8a, b), the values $\ell_m \approx 1.71$ and 1.86 are found for $U_r = 5.2$ and 5.5 respectively. Nevertheless, under plasma control (Fig. 8c, d)), the re-circulation region shortens in both cases to $\ell_m \approx 1.63$ and 1.71.

Figure 9 shows the averaged time and the fluctuations regarding the intensity of the velocity profiles for the *Plasma on* and *Plasma off* cases when $U_r = 5.5$ (similar results were found for $U_r = 5.2$). The profiles are taken at positions $x/D \in [1.00, 1.25, 1.50, 1.75]$. Consistent with the shortening of the re-circulation region by plasma actuation, a narrowing of the wake and accelerations of the upstream shear layer region can be observed in the averaged time velocity profiles $\langle u_x \rangle$ in Fig. 9 a). Besides, further downstream, plasma actuation produces a lower momentum deficit rather than unforced flows. The

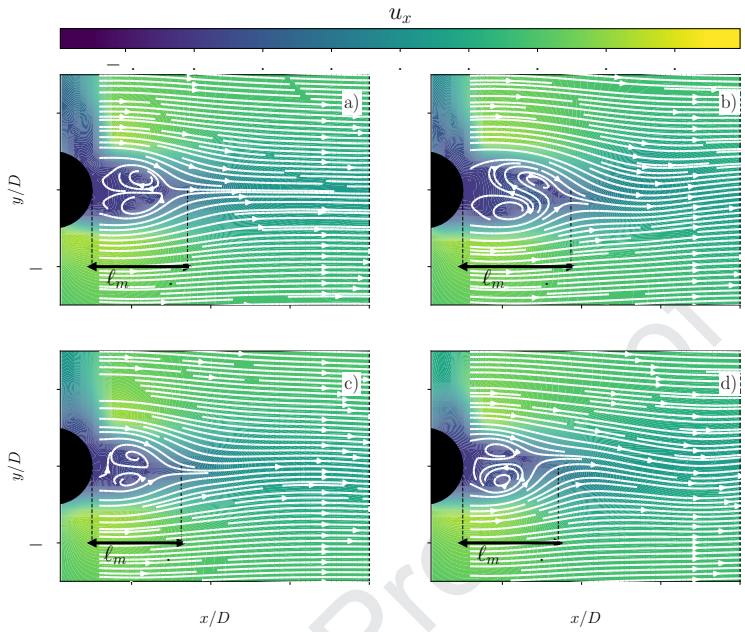

Figure 8: Streamlines and streamwise velocity u_x contours in m/s for a) $U_r = 5.2$ plasma off; b) $U_r = 5.5$ plasma off; c) $U_r = 5.2$ plasma on; d) $U_r = 5.5$ plasma on.

modification of re-circulation region is also accompanied by an increase in the Reynolds normal and shear stresses (Fig. 9b, c, d)), which corresponds to larger forces acting on a fictive control area enclosing the main re-circulation region.

3.2.1. Clustering technique

Since the PIV system is not resolved regarding time for the flow under consideration; to have relevant data of the dynamics of the flow, an indirect method was considered. As for forced flows, if a regular periodicity of the flow can be well established; for instance, when lock in regimes are attained, it is possible to synchronise the PIV acquisition with the actuator frequency in order to perform a phase average. However, under any other condition, it is not possible to predict the characteristic frequency of the flow and therefore it is not possible to perform a phase average acquisition. Thus, instead of relying on phase averaging techniques, a clustering technique, named *k-means* algorithm, was used

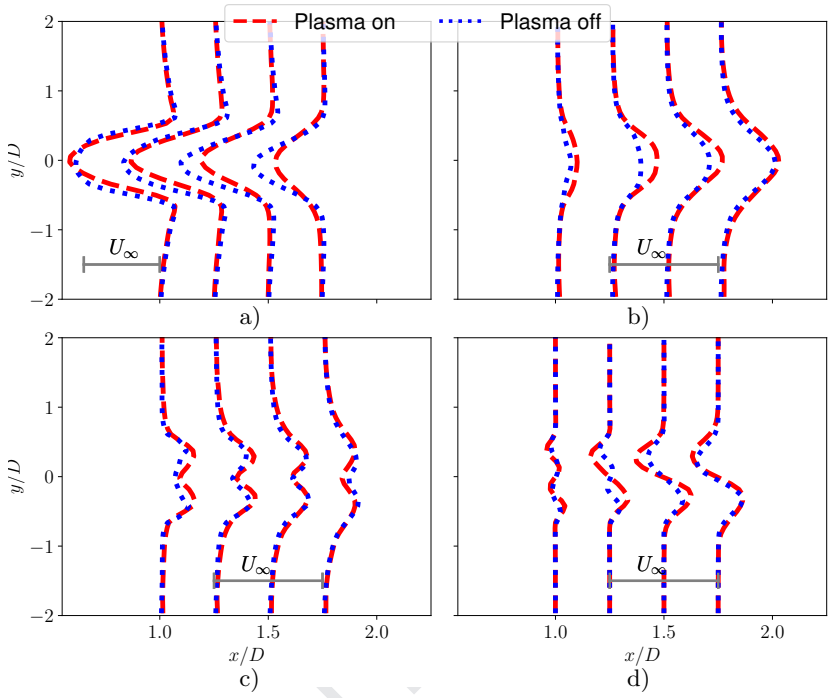

Figure 9: Time-averaged velocity moments profiles in $U_r = 5.5$. a): $\langle u_x \rangle$; b): transversal $\langle {u'_y}^2 \rangle^{1/2}$; c): streamwise $\langle {u'_x}^2 \rangle^{1/2}$; d): shear Reynolds stresses $\langle u'_x u'_y \rangle^{1/2}$. The profiles are taken at positions $x/D \in [1.00, 1.25, 1.50, 1.75]$.

to classify the acquired PIV fields and also to obtain a number of different representative states. A brief description of the applied algorithm can be found in [17], further details and extensions of this method are presented in [29].

In this investigation, each cluster or representative state of the flow was constructed from, at least, 12 snapshots. We considered, in this sense, a total of $N_c = 12$ clusters in order to obtain an insight of the flow dynamics of each studied case. Figure 10 shows vorticity contours for 6 clusters (numbered 0 to 5), that represent half of the vortex shedding period dynamics that corresponds to $U_r = 5.5$ without plasma control. By applying this method, the coherent structures, given by the BvK vortex street, become noticeable. The result, similar to phase averaging, allowed us to clearly identify vortex cores. The clusters are ordered through cross-correlation so shedding develops accordingly.

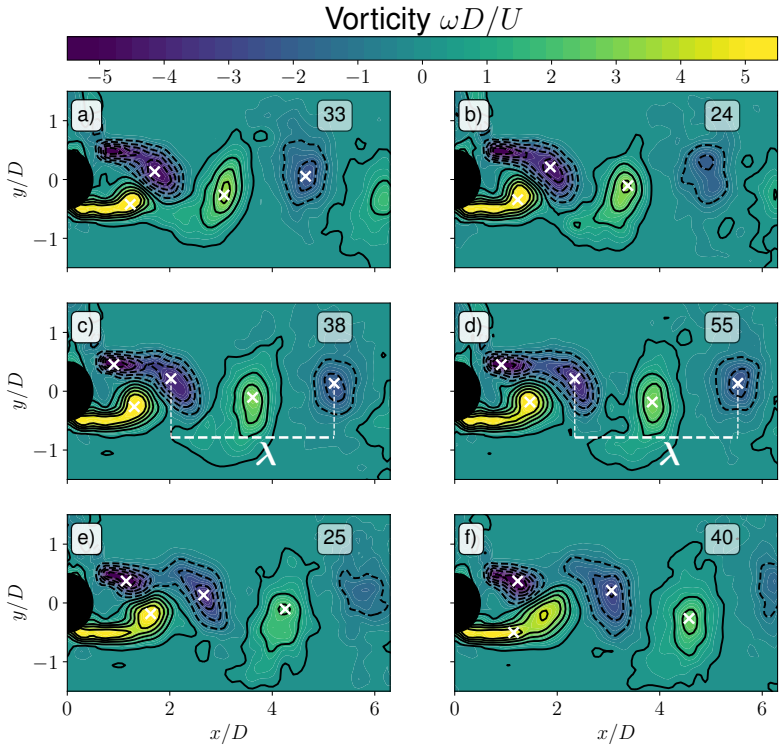

Figure 10: Dimensionless vorticity $\omega D/U$ contours of the clusters for $U_r = 5.5$, *Plasma off* case. The sequence from a) to f) corresponds to half a period of vortex shedding. The number of snapshots that belong to each cluster is shown at the upper left. Vortex cores are identified with a "×" symbol. An estimation of the BvK instability wavelength λ is shown.

Vortex identification for planar flows can be achieved by means of positive Q where $Q = (\partial u_i/\partial x_j)(\partial u_j/\partial x_i)/2$ is the second invariant of $\nabla \mathbf{u}$. By detecting local minima, we have marked the cores and a wavelength λ can be estimated. For $U_r = 5.5$, $\lambda \simeq 3.3$ without flow control. In the same sense, Fig. 11 shows the clusters for $U_r = 5.5$ with plasma control. It is clearly observed that BvK vortex street remains the same as the coherent structure. The wavelength is slightly smaller, as $\lambda \simeq 3.0$.

Previous articles shown that the electrohydrodynamic forcing with electrodes similarly placed produce a reduction of the main base pressure [4]. This result

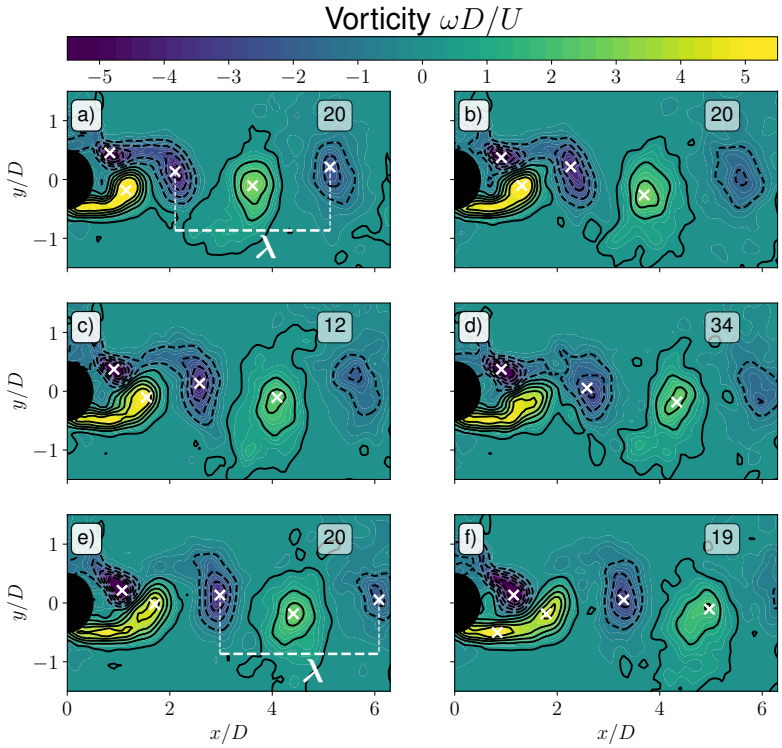

Figure 11: Dimensionless vorticity $\omega D/U$ contours of the cluster sequences of half a period in the *Plasma on* case for $U_r = 5.5$. The number of snapshots that belong to each cluster is shown at the upper left. Vortex cores are identified with a "×" symbol. An estimation of the BvK instability wavelength λ is shown in a) and e).

was obtained in agreement with other authors' observations, demonstrating that a signal forcing with this kind of plasma actuator in a similar configuration promotes the dimensionality of the flow [36]. This leads to vortex of higher intensity and, in consequence, to an increase on the forces produced by the flow on the structure. Accordingly, we can not associate the suppression of vibrations of the cylinder to a reduction of the intensity of the forcing (vortex-strength-reduction mechanism). The only possible mechanism can be a shifting of the vortex shedding frequency away from the natural frequency of the structure.

The flow can not be driven in this case by the very high frequency of the

plasma and the only possible mechanism to modify the shedding frequency is an alteration of the flow instabilities phenomena associated with the vortices formation. In order to analyse possible changes in the frequency of vortex shedding as a consequence of actuation, we rely on the PIV measurements. The time averaged flow fields show significant modifications when control is on. A linear instability analysis was proposed here to analyse how the vortex shedding frequencies could be modified. However, it becomes much more appropriate to determine it from experiments. Given that wave velocity $c = \lambda f$ can be retrieved from clusters velocity fields, a straightforward measure of vortex frequency can be obtained. So, when no control is applied, the Strouhal number is $St = 0.19 \pm 0.1$ while when plasma forces the wake, the number is $St = 0.25 \pm 0.1$.

These results are consistent with the observed increase in frequency and subsequent shortening of the re-circulation length observed regarding the flow regime analysed when increasing the free stream velocity. Thus, the mechanism of frequency shift promoted by alterations of the base flow (mean flow) is compatible with the results we have obtained and enables us to explain the suppression of VIV produced by the plasma actuation.

4. Conclusions

The plasma forcing of the vortex induced vibrating cylinder leads to a shorter vortex formation region compared with the case without control. The modification of re-circulation region is accompanied by an increase of the Reynolds normal and shear stresses, which corresponds to larger forces acting on a fictive control area enclosing the main re-circulation region. The altered topology of the vortex formation region is accompanied by a significant change on the vortex shedding frequency which results in a total suppression of the VIV.

The intensities of the vortices that force the structure were not decreased by the actuation. The attenuation produced by the actuation can be observed in the range of frequencies of the natural vortex shedding phenomena. This is a consequence of the modifications occurred to the process of development of

instabilities of the flow that is determined by the alterations produced on the main base flow.

The "high" frequency of the plasma actuation was not significantly observed in the "slow" dynamic behaviour of the system we studied. However, the frequency of this actuation may couple at larger Reynolds number with the vortex shedding frequency or with the one of the transition eddies. Operation of plasma actuators in the "burst mode" could also enable us to introduce coupling at lower frequencies. Future studies should focus on achieving the possibility to drive the flow with the frequency of the actuators and analyse the possibility to increase or suppress VIV under these circumstances.

Finally, the structure we considered in this study even not flexible, may vibrate in different modes and our strategy was to act on the flow and not directly on the structure. The kind of actuator we proposed can be tuned to excite the flow with different frequencies, that may go from a few Hz to tenths of kHz. The possibility to extend the control we proposed to flexible structures, will depend not only on the time domain but also on the spatial scale of the problem. However, the strategy proposed only seems suitable for cases in which the structures will not be largely deformed by the fluid structure interaction.

References

[1] Al-Sadawi, L., Chong, T.P., Kim, J.H., 2019. Aerodynamic noise reduction by plasma actuators for a flat plate with blunt trailing edge. J. Sound Vib. 439, 173–93. doi:10.1016/j.jsv.2018.08.029.

[2] Artana, G., D'Adamo, J., Leger, L., Moreau, E., Touchard, G., 2002. Flow control with electrohydrodynamic actuators. AIAA Journal 9, 1773–9. doi:10.2514/2.1882. american Institute of Aeronautics and Astronautics.

[3] Artana, G., Desimone, G., Touchard, G., 1999. Study of the changes in the flow around a cylinder caused by electroconvection, in: Taylor, D.M. (Ed.), Electrostatics 1999, Proceedings of the 10th International Confer-

ence, Cambridge, UK, 28-31 March 1999, Institute of Physics Conference, Series Number 163. CRC Press. pp. 147–52.

[4] Artana, G., Sosa, R., Moreau, E., Touchard, G., 2003. Control of the near-wake flow around a circular cylinder with electrohydrodynamic actuators. Exp. Fluids 35, 580–8. doi:10.1007/s00348-003-0704-z.

[5] Barkley, D., 2006. Linear analysis of the cylinder wake mean flow. EPL 75, 750. doi:10.1209/epl/i2006-10168-7.

[6] Bearman, P., 2011. Circular cylinder wakes and vortex-induced vibrations. J. Fluid Struct. 27, 648–58. doi:10.1016/j.jfluidstructs.2011.03.021. exported from https://app.dimensions.ai on 2019/04/12.

[7] Bearman, P.W., 1984. Vortex shedding from oscillating bluff bodies. Annu. Rev. Fluid Mech. 16, 195–222. doi:10.1146/annurev.fl.16.010184.001211.

[8] Bearman, P.W., Brankovic, M., 2004. Experimental studies of passive control of vortex-induced vibration. Eur. J. Mech. B Fluids 23, 9–15. doi:10.1016/j.euromechflu.2003.06.002.

[9] Benard, N., Moreau, E., 2010. Capabilities of the dielectric barrier discharge plasma actuator for multi-frequency excitations. J. Phys. D Appl. Phys. 43, 145201.

[10] Blevins, R.D., 1990. Flow-induced Vibration. 2nd ed ed., Kreiger Publisher Company.

[11] Brankovic, M., Bearman, P.W., 2006. Measurements of transverse forces on circular cylinders undergoing vortex-induced vibration. J. Fluid Struct. 22, 829–36. doi:10.1016/j.jfluidstructs.2006.04.022.

[12] Cattafesta, L.N., Sheplak, M., 2011. Actuators for active flow control. Annu. Rev. Fluid Mech. 43, 247–72. doi:10.1146/annurev-fluid-122109-160634.

[13] Chen, W.L., Li, H., Hu, H., 2014. An experimental study on a suction flow control method to reduce the unsteadiness of the wind loads acting on a circular cylinder. Exp. Fluids 55. doi:10.1007/s00348-014-1707-7.

[14] Chen, Z., Aubry, N., 2005. Closed-loop control of vortex-induced vibration. Comm. Nonlinear Sci. Numer Simulat. 10, 287–97. doi:10.1016/S1007-5704(03)00127-8.

[15] Choi, H., Jeon, W.P., Kim, J., 2008. Control of flow over a bluff body. Annu. Rev. Fluid Mech. 40, 113–39. doi:10.1146/annurev.fluid.39.050905.110149.

[16] Corke, T.C., Enloe, C.L., Wilkinson, S.P., 2010. Dielectric barrier discharge plasma actuators for flow control. Annu. Rev. Fluid Mech. 42, 505–29. doi:10.1146/annurev-fluid-121108-145550.

[17] D'Adamo, J., Leonardo, L., Castro Hebrero, F., Sosa, R., Duriez, T., Artana, G., 2017. Circular cylinder drag reduction by three-electrode plasma symmetric forcing. J. Fluids Eng. Published Monyhly by ASME 139, 061202–1/14. doi:10.1115/1.4035947.

[18] Du, L., Sun, X., 2015. Suppression of vortex-induced vibration using the rotary oscillation of a cylinder. Phys. Fluids 27. doi:10.1063/1.4913353.

[19] Dušek, J., Gal, P.L., Frauni, P., 1994. A numerical and theoretical study of the first hopf bifurcation in a cylinder wake. Fluid Mech. 264, 59–80. doi:10.1017/S0022112094000583.

[20] Feng, C., 1968. The measurements of vortex-induced effects in flow past a stationary and oscillating circular and D-section cylinders. Master's thesis. University of British Columbia, Vancouver, Canada. Masters thesis in the Department of Mechanical Engineering.

[21] Fey, U., Konig, M., Eckelmann, H., 1998. A new strouhal reynolds number relationship for the circular cylinder in the range $47 < \mathrm{Re} < 2 \cdot 10^5$. Phys. Fluids 10, 1547–9. doi:10.1063/1.869675.

[22] Gabbai, R.D., Benaroya, H., 2005. An overview of modeling and experiments of vortex-induced vibration of circular cylinders. J. Sound Vib. 282, 575–616. doi:10.1016/j.jsv.2004.04.017.

[23] Gad-el Hak, M., 2000. Flow Control: Passive, Active, and Reactive Flow Management. Cambridge University Press. doi:10.1017/CBO9780511529535.

[24] Hover, F.S., Tvedt, H., Triantafyllou, M.S., 2001. Vortex-induced vibrations of a cylinder with tripping wires. Fluid Mech. 448, 175–95. doi:10.1017/S0022112001005985.

[25] Huang, X., Zhang, X., 2008. Streamwise and spanwise plasma actuators for flow-induced cavity noise control. Phys. Fluids 20, 037101. doi:10.1063/1.2890448.

[26] Huang, X., Zhang, X., Li, Y., 2010. Broadband flow-induced sound control using plasma actuators. J. Sound Vib. 329, 2477–89. doi:10.1016/j.jsv.2010.01.018.

[27] Jauvtis, N., Williamson, C.H.K., 2004. The effect of two degrees of freedom on vortex-induced vibration at low mass and damping. Fluid Mech. 509, 23–62. doi:10.1017/S0022112004008778.

[28] Jayaraman, B., Thakur, S., Shyy, T., 2007. Modeling of fluid dynamics and heat transfer induced by dielectric barrier plasma actuator. J. Heat Transfer. 129, 517–25. doi:10.1115/1.2709659.

[29] Kaiser, E., Noack, B., Cordier, L., Spohn, A., Segond, M., Abel, M., Daviller, G., Osth, J., S., K., K., N.R., 2014. Cluster-based reduced-order modelling of a mixing layer. Fluid Mech. 754, 365–414. doi:10.1017/jfm.2014.355.

[30] Kopiev, V.F., Kazansky, P.N., Kopiev, V.A., Moralev, I.A., Zaytsev, M.Y., 2017. Hf dbd plasma actuators for reduction of cylinder noise in flow. J. Phys. D Appl. Phys. 50, 475204. doi:10.1088/1361-6463/aa91aa.

[31] Korkischko, I., Meneghini, J.R., 2010. Experimental investigation of flow-induced vibration on isolated and tandem circular cylinders fitted with strakes. J. Fluid Struct. 26, 611–25. doi:10.1016/j.jfluidstructs.2010.03.001.

[32] Korkischko, I., Meneghini, J.R., 2012. Suppression of vortex-induced vibration using moving surface boundary-layer control. J. Fluid Struct. 34, 259–70. doi:10.1016/j.jfluidstructs.2012.05.010.

[33] Loeb, L.B., 1939. Fundamental Processes of Electrical Discharge in Gases. John Wiley & Sons. doi:10.1038/146729a0.

[34] Mittal, S., Kumar, V., 2001. Flow-induced vibrations of a light circular cylinder at reynolds numbers 10^3 to 10^4. J. Sound Vib. 245, 923–946. doi:10.1006/jsvi.2001.3612.

[35] Moreau, E., 2007. Airflow control by non-thermal plasma actuators. J. Phys. D Appl. Phys. 40, 605. doi:10.1088/0022-3727/40/3/S01.

[36] Munska, M.D., McLaughlin, T.E., 2005. Circular cylinder flow control using plasma actuators. 43rd AIAA Aerospace Sciences Meeting and Exhibit, Aerospace Sciences Meetings AIAA 2005-141. doi:10.2514/6.2005-141. aerospace Sciences Meetings, 10 - 13 January 2005, Reno, Nevada.

[37] Roth, J.R., Sherman, D.M., Wilkinson, S.P., 2000. Electrohydrodynamic flow control with a glow-discharge surface plasma. AIAA Journal 38, 1166–72. doi:10.2514/2.1110.

[38] Sari, G., Mureithi, N.W., 2010. Active control of vortex induced vibration by plasma actuation. ASME Proceedings, 7th International Symposium on Fluid-Structure Interactions, Flow-Sound Interactions, and Flow-Induced Vibration and Noise 3, 1079–87. doi:10.1115/FEDSM-ICNMM2010-30515. paper No. FEDSM-ICNMM2010-30515.

[39] Sarpkaya, T., 2004. A critical review of the intrinsic nature of vortex-induced vibrations. J. Fluid Struct. 19, 389–447. doi:10.1016/j.jfluidstructs.2004.02.005.

[40] Skaugset, K.B., Larsen, C.M., 2003. Direct numerical simulation and experimental investigation on suppression of vortex induced vibrations of circular cylinders by radial water jets. Flow Tutbul. Combust. 71, 35–59. doi:10.1023/B:APPL.0000014924.80246.e4.

[41] Sumer, B., Fredsoe, J., 2006. Hydrodynamics Around Cylindrical Structures. volume 26 of *Advanced Series on Ocean Engineering*. World scientific ed., World Scientific. doi:https://doi.org/10.1142/6248.

[42] Thomas, F.O., Kozlov, A., Corke, T.C., 2008. Plasma actuators for cylinder flow control and noise reduction. AIAA journal 46, 1921–31. doi:10.2514/1.27821.

[43] Trim, A.D., Braaten, H., Lie, H., Tognarelli, M.A., 2005. Experimental investigation of vortex-induced vibration of long marine risers. J. Fluid Struct. 21, 335–61. doi:10.1016/j.jfluidstructs.2005.07.014.

[44] Wang, C., Tang, H., Duan, F., Yu, S.C.M., 2016a. Control of wakes and vortex-induced vibrations of a single circular cylinder using synthetic jets. J. Fluid Struct. 60, 160–79. doi:10.1016/j.jfluidstructs.2015.11.003.

[45] Wang, C., Tang, H., Yu, S., Duan, F., 2016b. Active control of vortex-induced vibrations of a circular cylinder using windward-suction-leeward-blowing actuation. Phys. Fluids 28. doi:10.1063/1.4947246.

[46] Wang, C., Tang, H., Yu, S.C.M., Duan, F., 2017. Control of vortex-induced vibration using a pair of synthetic jets: Influence of active lock-on. Phys. Fluids 29. doi:10.1063/1.4996231.

[47] Wang, J.J., Choi, K.S., Feng, L.H., Jukes, T.N., Whalley, R.D., 2013. Recent developments in dbd plasma flow control. Prog. Aerosp. Sci. 62, 52–78. doi:10.1016/j.paerosci.2013.05.003.

[48] Willden, R.H.J., Graham, J.M.R., 2006. Three distinct response regimes for the transverse vortex-induced vibrations of circular cylinders at low reynolds numbers. J. Fluid Struct. 22, 885–95. doi:10.1016/j.jfluidstructs.2006.04.005.

[49] Williamson, C.H.K., 1996. Vortex dynamics in the cylinder wake. Annu. Rev. Fluid Mech. 28, 477–539. doi:10.1146/annurev.fl.28.010196.002401.

[50] Williamson, C.H.K., Goverdhan, R., 2004. Vortex induced vibrations. Annu. Rev. Fluid Mech. 36, 413–55. doi:doi.org/10.1146/annurev.fluid.36.050802.122128.

[51] Williamson, C.H.K., Goverdhan, R., 2008. A brief review of recent results in vortex-induced vibrations. J. Wind. Eng. Ind. Aerod. 96, 713–35. doi:doi.org/10.1016/j.jweia.2007.06.019.

[52] Xu, F., Chen, W.L., Xiao, Y.Q., Li, H., Ou, J.P., 2014. Numerical study on the suppression of the vortex-induced vibration of an elastically mounted cylinder by a traveling wave wall. J. Fluid Struct. 44, 145–65. doi:10.1016/j.jfluidstructs.2013.10.005.

[53] Zdravkovich, M.M., 1981. Review and classification of various aerodynamic and hydrodynamic means for suppressing vortex shedding. J. Wind. Eng. Ind. Aerod. 7, 145–89. doi:10.1016/0167-6105(81)90036-2.

[54] Zhang, M., Cheng, L., Zhou, Y., 2004. Closed-loop-controlled vortex shedding and vibration of a flexibly supported square cylinder under different schemes. Phys. Fluids 16, 1439–48. doi:10.1063/1.1687413.

F. Castro Hebrero: Methodology, Validation, Writing - Original Draft.

J. D´Adamo: Software , Data Curation, Visualization.

R. Sosa: Conceptualization, Formal analysis , Writing - Review & Editing.

G. Artana: Project administration, Investigation, Supervision, Funding acquisition, Resources

Declaration of interests

X The authors declare that they have no known competing financialinterestsor personal relationships that could have appeared to influence the work reported in this paper.

☐ The authors declare the following financial interests/personal relationships which may be considered as potential competing interests: